generalizing the findings beyond the theoretical context of (*6*), which focused on the benefits of social interaction. Indeed, predictions from SCM were confirmed for a within-individual design: When participants responded to 2AFC items on several occasions, they were more confident when they made their more frequent decision than when they made their less frequent decision (*7*–*9*). The tasks used in study 3 were presented twice with a 1-week interval. The hypothesis tested is that a compilation of the high-confidence choices across the two presentations should yield the same pattern of results as that observed for a between-person compilation.

The extension of the wisdom-of-crowds idea to a within-person context (*26*–*28*) indicated that when participants estimated a quantity on two occasions, their average estimate was closer to the truth than their individual estimates. Therefore, in Study 5 *D-HC* performance was compared with average performance (*AP*) across the two sessions. The items were classified as CC or CW by using the same classification as in (*8*) and in study 3. Between-session differences in confidence were first nullified by setting the mean and SD of confidence judgments in session 2 as those of session 1 for each task and participant. For each item, the response associated with higher confidence across the two sessions was slated to *D-HC* and the other to *D-LC*. Mean percent correct for *D-HC*, *D-LC*, and *AP* is presented in Table 2 for the CC and CW items in each task.

A three-way ANOVA, task (Shapes versus Lines) × measure (*D-HC* versus *AP*) × item type (CC versus CW) yielded $F_{1,49} = 5.03$, MSE = 24.83, $P < 0.05$ for the measure × item type interaction. For the CC items, *D-HC* accuracy (82.54%) was higher than *AP* accuracy (81.24%) [$t(49) = 2.67$, $P < 0.05$]. For the CW items, *D-HC* accuracy (24.06%) tended to be somewhat lower than *AP* accuracy (25.00%) [$t(49) = 1.05$, $P < 0.31$]. In addition, across the CC items, confidence was higher when the correct choice was made than when the wrong choice was made, whereas the opposite was true for the CW items.

A comparison of *D-HC* with *D-LC* suggests that the benefit from the MCS algorithm in the case of CC items was more limited for the within-person confidence-based slating (study 5; 2.68 percentage points) than for the cross-person slating (study 3; 6.62 percentage points). The reason derives from the greater independence between decisions of two members of a dyad (study 3; a correlation of 0.02) than between the two decisions of the same person (study 5; a correlation of 0.63) (*28*).

The present work delivers three messages. First, under many conditions in which participants' decisions are correct by and large, a 2HBT1 effect should be observed. The results of the present study are consistent with Bahrami *et al.*'s (*6*) proposition that the benefit from dyadic interaction derives from individuals communicating their level of confidence accurately to each other. Here, however, a 2HBT1 effect was observed (studies 1 and 2) in the absence of social interaction. The selection of responses on the basis of confidence improved accuracy beyond the improvement achieved by the aggregation of responses across individuals (*15*).

Second, however, in situations in which most participants tend to make the wrong decisions, the MCS algorithm, as well as social interaction, is expected to yield group decisions that are even less accurate than those of each individual alone. In such cases, it is the low-confidence individuals who are more likely to be correct, and reliance on the more confident members should lead the group astray.

Last, the within-individual results (study 5) highlight a general perspective for the analysis of decision accuracy that goes beyond the effects of social interaction (*6*). This perspective, as captured by SCM, involves the variations in confidence that occur both within individuals and between individuals when choice and confidence are based on the sampling of clues from a common database (*7*, *27*).

References and Notes

1. R. S. Baron, in *Advances in Experimental Social Psychology*, M. P. Zanna, Ed. (Elsevier Academic Press, San Diego, CA, 2005), pp. 219–253.
2. J. K. Esser, *Organ. Behav. Hum. Decis. Process.* **73**, 116 (1998).
3. I. Janis, Ed., *Groupthink: A Psychological Study of Policy Decisions and Fiascos* (Houghton Mifflin, Boston, 1982).
4. G. W. Hill, *Psychol. Bull.* **91**, 517 (1982).
5. P. R. Laughlin, E. C. Hatch, J. S. Silver, L. Boh, *J. Pers. Soc. Psychol.* **90**, 644 (2006).
6. B. Bahrami *et al.*, *Science* **329**, 1081 (2010).
7. A. Koriat, *Psychol. Rev.* **119**, 80 (2012).
8. A. Koriat, *J. Exp. Psychol. Gen.* **140**, 117 (2011).
9. A. Koriat, S. Adiv, *Soc. Cogn.* **29**, 577 (2011).
10. J. Dunlosky, J. Metcalfe, *Metacognition* (Sage, Thousand Oaks, CA, 2009)
11. A. Koriat, *J. Exp. Psychol. Learn. Mem. Cogn.* **34**, 945 (2008).
12. W. F. Brewer, C. Sampaio, *Memory* **14**, 540 (2006).
13. A. Koriat, *Mem. Cognit.* **4**, 244 (1976).
14. A. Koriat, *J. Exp. Psychol. Gen.* **124**, 311 (1995).
15. D. Ariely *et al.*, *J. Exp. Psychol. Appl.* **6**, 130 (2000).
16. R. Clemen, *Int. J. Forecast.* **5**, 559 (1989).
17. J. Surowiecki, *The Wisdom of Crowds* (Anchor Books, New York, 2005).
18. T. S. Wallsten, A. Diederich, *Math. Soc. Sci.* **41**, 1 (2001).
19. For a popular presentation, see (*29*).
20. D. Kahneman, *Thinking Fast and Slow* (Farrar, Straus & Giroux, New York, 2011).
21. B. L. Cutler, S. D. Penrod, T. E. Stuve, *Law Hum. Behav.* **12**, 41 (1988).
22. Z. L. Tormala, D. D. Rucker, *Soc. Personal. Psychol. Compa.* **1**, 469 (2007).
23. K. Kleitman, L. Stankov, *Appl. Cogn. Psychol.* **15**, 321 (2001).
24. Materials and methods, and additional analyses, are available as supplementary materials on *Science* Online.
25. M. K. Dhami, R. Hertwig, U. Hoffrage, *Psychol. Bull.* **130**, 959 (2004).
26. S. M. Herzog, R. Hertwig, *Psychol. Sci.* **20**, 231 (2009).
27. K. L. Hourihan, A. S. Benjamin, *J. Exp. Psychol. Learn. Mem. Cogn.* **36**, 1068 (2010).
28. E. Vul, H. Pashler, *Psychol. Sci.* **19**, 645 (2008).
29. R. Burton, *On Being Certain: Believing You Are Right Even When You're Not* (St. Martin's Press, New York, 2008).

Acknowledgments: I am grateful to R. Gil and D. Klein for their help in the analyses of the results, and to S. Adiv for her assistance in the preparation of the article. Support for this project was received from the Max Wertheimer Minerva Center for Cognitive Processes and Human Performance, University of Haifa.

Suppplementary Materials

www.sciencemag.org/cgi/content/full/336/6079/360/DC1
Materials and Methods
SOM Text
Table S1
References

14 November 2011; accepted 29 February 2012
10.1126/science.1216549

Structure of an Intermediate State in Protein Folding and Aggregation

Philipp Neudecker,[1,2,3,4,5] Paul Robustelli,[6] Andrea Cavalli,[6] Patrick Walsh,[1,7] Patrik Lundström,[1,2,3] Arash Zarrine-Afsar,[1,2] Simon Sharpe,[1,7] Michele Vendruscolo,[6] Lewis E. Kay[1,2,3,7]*

Protein-folding intermediates have been implicated in amyloid fibril formation involved in neurodegenerative disorders. However, the structural mechanisms by which intermediates initiate fibrillar aggregation have remained largely elusive. To gain insight, we used relaxation dispersion nuclear magnetic resonance spectroscopy to determine the structure of a low-populated, on-pathway folding intermediate of the A39V/N53P/V55L (A, Ala; V, Val; N, Asn; P, Pro; L, Leu) Fyn SH3 domain. The carboxyl terminus remains disordered in this intermediate, thereby exposing the aggregation-prone amino-terminal β strand. Accordingly, mutants lacking the carboxyl terminus and thus mimicking the intermediate fail to safeguard the folding route and spontaneously form fibrillar aggregates. The structure provides a detailed characterization of the non-native interactions stabilizing an aggregation-prone intermediate under native conditions and insight into how such an intermediate can derail folding and initiate fibrillation.

Insoluble β sheet–rich fibrillar aggregates, called amyloid fibrils, form conspicuous deposits in tissue associated with a wide range of human pathologies, including Alzheimer's and Parkinson's diseases and type 2 diabetes (*1*–*4*). Fibril formation has been reported for many

proteins, and aggregates are often highly cytotoxic, even for proteins not linked directly to a clinical condition, as in the case of SH3 domains (*5*).

Although experimentally determined atomic-resolution models have started to appear for amyloid fibrils (*6*), the detailed structural mechanisms of aggregation, generally believed to follow nucleation-and-growth schemes (*3*), are still largely unclear. Initial observations that amyloid formation often occurs for disordered or destabilized polypeptide chains suggested that aggregation requires extensive unfolding (*7*). However, fibril formation is also observed for globular proteins under native conditions, and theoretical considerations as well as experimental evidence indicate that aggregation proceeds via native-like intermediates that are formed after the major folding barrier in many of these systems (*4*). Reports that pre- and protofibrillar oligomers are often as or even more cytotoxic than the fibrils themselves (*3*, *5*, *8*–*10*) have increasingly shifted focus toward early stages of aggregation and fibril formation. Recently, an intermediate with a non-native *trans*-proline conformation was identified as the direct precursor of β-2-microglobulin fibril elongation under native conditions (*11*). The structure of this intermediate, although not known in detail, is close to the native state (*11*). A mutant enforcing the trans conformation crystallized directly as a crystallographic dimer, suggesting a straightforward model for monomer arrangement within a fibril (*12*).

Because the experimental detection and characterization of low-populated, transiently formed intermediates in protein folding and aggregation is challenging (*13*, *14*), their atomic-resolution structures, aggregation propensities, and roles in aggregation are not understood in detail. With the development of Carr-Purcell-Meiboom-Gill (CPMG) relaxation dispersion nuclear magnetic resonance (RD NMR) spectroscopy (fig. S1) (*15*), however, protein-folding exchange reactions on the millisecond time scale can be studied at atomic resolution and under native equilibrium conditions (*16*). In addition to quantifying the kinetics and thermodynamics of the exchange process, backbone chemical shifts and bond vector orientations of low-populated (excited) states can be obtained, which are key to the atomic-resolution structure determination of these transient conformers (*17*, *18*).

In previous ^{15}N CPMG RD NMR studies (*16*, *19*), we demonstrated that the A39V/N53P/V55L (A, Ala; V, Val; N, Asn; P, Pro; L, Leu) Fyn SH3 domain folds from the unfolded state (U) via an on-pathway, low-populated (≈2%) intermediate (I) to a native β-sandwich fold (N). The stability and folding kinetics of this mutant are well within the window of the CPMG method (fig. S1). In the structure of the A39V/N53P/

[1]Department of Biochemistry, University of Toronto, Toronto, Ontario M5S 1A8, Canada. [2]Department of Chemistry, University of Toronto, Toronto, Ontario M5S 3H6, Canada. [3]Department of Molecular Genetics, University of Toronto, Toronto, Ontario M5S 1A8, Canada. [4]Institut für Physikalische Biologie, Heinrich-Heine-Universität, 40225 Düsseldorf, Germany. [5]ICS-6 (Strukturbiochemie), Forschungszentrum Jülich, 52425 Jülich, Germany. [6]Department of Chemistry, University of Cambridge, Cambridge, CB2 1EW, UK. [7]Program in Molecular Structure and Function, Hospital for Sick Children, Toronto, Ontario M5G 1X8, Canada.

*To whom correspondence should be addressed. E-mail: kay@pound.med.utoronto.ca

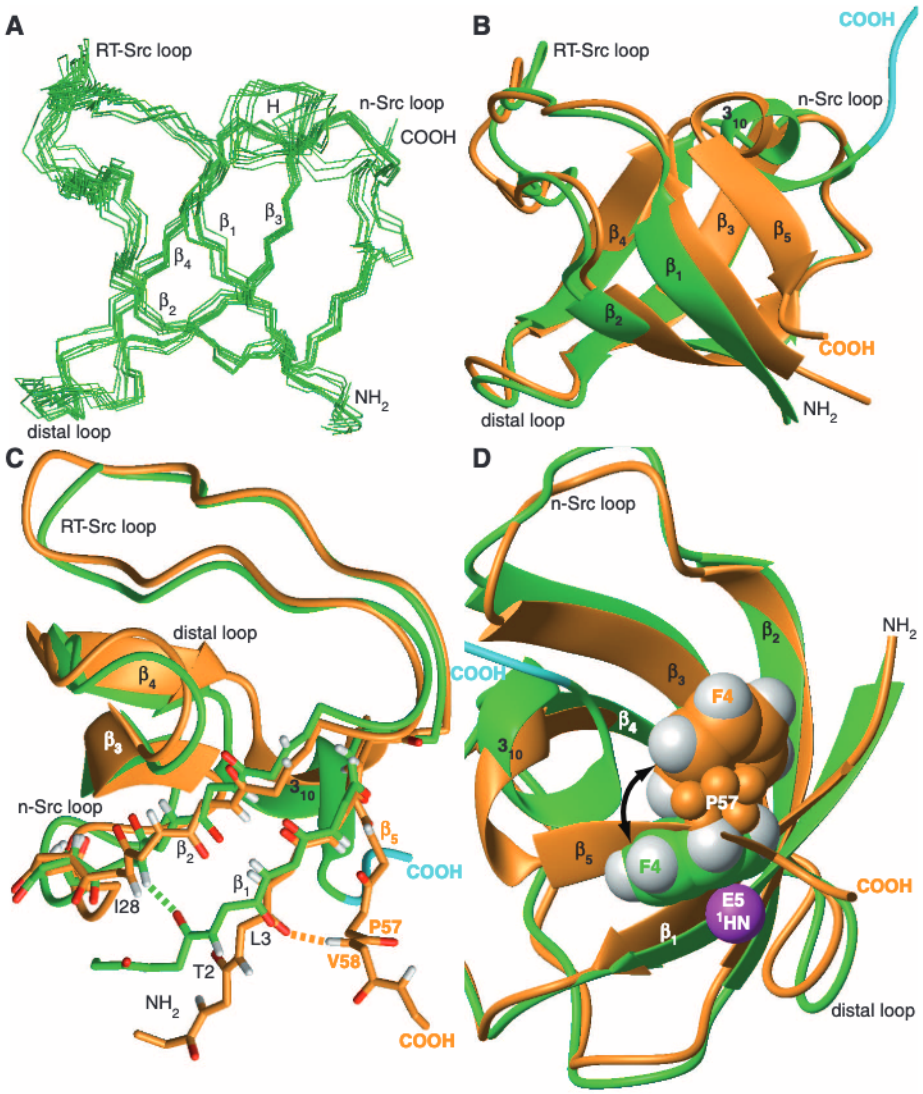

Fig. 1. Structure of the low-populated intermediate. **(A)** Backbone overlay of the 10 lowest-energy structures of the intermediate of A39V/N53P/V55L Fyn SH3 from Ser[1] to Ala[56]. **(B)** Backbone overlay in schematic representation of the lowest-energy solution structure of the native state (orange) (fig. S2 and table S1) with the lowest-energy solution structure of the intermediate state (green). Residues Pro[57] to Asp[59], which are completely flexible as established by random-coil chemical shifts (fig. S5B), have been added in an extended conformation for illustrative purposes only and are highlighted in light blue. **(C)** Same overlay as in (B) illustrating the differences in hydrogen bonding (dashed lines) between strands β_5, β_1, and β_2. **(D)** Overlay as in (B) and (C) illustrating how the side chain of Phe[4] (F4) (space-filling representation) stacks with Pro[57] (P57) (ball-and-stick representation) in the native state but fills the gap left by the missing strand β_5 in the intermediate. The amide proton of Glu[5] (E5) is shown in magenta.

V55L Fyn SH3 domain native state, determined from NMR data starting from the crystal structure of the N53I/V55L Fyn SH3 domain (*20*) (fig. S2 and table S1), the terminal (strands β_1 and β_5) and central (strands β_2, β_3, and β_4) β sheets are connected at one edge by hydrogen bonds between β_1 and β_2 to form a five-stranded incomplete antiparallel β barrel (Fig. 1). The I state is a compact near-native intermediate formed after the major folding barrier (*19*), with the central three-stranded β sheet already intact in the rate-limiting transition state between U and I (*19*, *21*, *22*). Interestingly, the ^{15}N chemical shifts of the intermediate revealed pronounced non-native interactions (fig. S3) (*19*, *22*). Contrary to the notion that such interactions cause kinetic traps that evolution has largely selected against, there is increasing evidence that they play an important role in the folding and misfolding of many proteins (*4*, *14*, *20*, *23*), including the Fyn SH3 domain (*20*). To gain further insight into how non-native interactions influence both folding and misfolding, we used CPMG RD NMR spectroscopy under solution conditions that favor the native state to determine the three-dimensional structure of the transient intermediate of the A39V/N53P/V55L Fyn SH3 domain (see supplementary materials and methods).

To this end, we recorded and analyzed a variety of CPMG RD experiments (fig. S4) on several suitably isotope-labeled A39V/N53P/V55L Fyn SH3 samples at 20°C. ^{15}N, ^{1}HN, ^{13}CO, ^{13}Cα, and ^{1}Hα backbone chemical shifts of the intermediate (fig. S3B), ^{15}N-^{1}HN backbone amide residual dipolar couplings, and ^{13}CO residual chemical shift anisotropies were obtained from fits of the resulting RD profiles from sites showing chemical exchange (fig. S4). The extracted chemical shifts corroborate our earlier observations (*19*, *22*) that much of the native backbone fold is already formed in I, except for the N- and C-terminal regions (fig. S5A), but provide substantially more data on which to base a structural analysis so that the conformational changes to the N and C termini can be elucidated. Most notably, the C terminus from Pro^{57} to Asp^{59} is disordered in I (fig. S5B), which implies that strand β_5 is not formed. We used the CamShift chemical shift restrained molecular dynamics structure calculation protocol (figs. S6 to S8) (*24*), which makes use of RD-derived backbone chemical shifts, ^{15}N-^{1}HN residual dipolar couplings, and ^{13}CO residual chemical shift anisotropies, to obtain more quantitative structural information about the well-ordered part of the domain.

Superposition of the 10 resulting lowest-energy structures of the folding intermediate (Fig. 1A) reveals that the topology of strands β_1 to β_4 followed by the helical turn is native-like (Fig. 1B; see table S2 for structural statistics), in agreement with backbone amide H/D exchange experiments (fig. S9). The tertiary interactions missing in the absence of strand β_5 are partially compensated for by non-native contacts within this residual native-like backbone topology. In particular, strand β_1 compensates for the loss of hydrogen bonding to β_5 by associating more tightly with strand β_2 through the formation of a non-native hydrogen bond between Ile^{28} HN and Thr^{2} CO (Fig. 1C), with a much shorter HN-O distance in the intermediate (1.92 ± 0.08 Å) relative to the native structure (4.39 ± 0.28 Å). In addition, the four-stranded β sheet of I is stabilized by non-native hydrophobic core packing with the bulky aromatic ring of Phe^{4} filling the space occupied by the backbone of strand β_5 in the native state (Fig. 1D). An advantage of the chemical shift restrained structure calculation is the possibility to determine side-chain conformations by exploiting aromatic-ring current effects on nearby backbone atom chemical shifts. The difference in aromatic packing between states N and I is associated with large chemical shift changes affecting the amide proton of Glu^{5} (Fig. 1D and fig. S3) and other backbone resonances; this enables reliable placement of the aromatic side chain of Phe^{4} in a position that is consistent with backbone amide H/D exchange measurements (fig. S9).

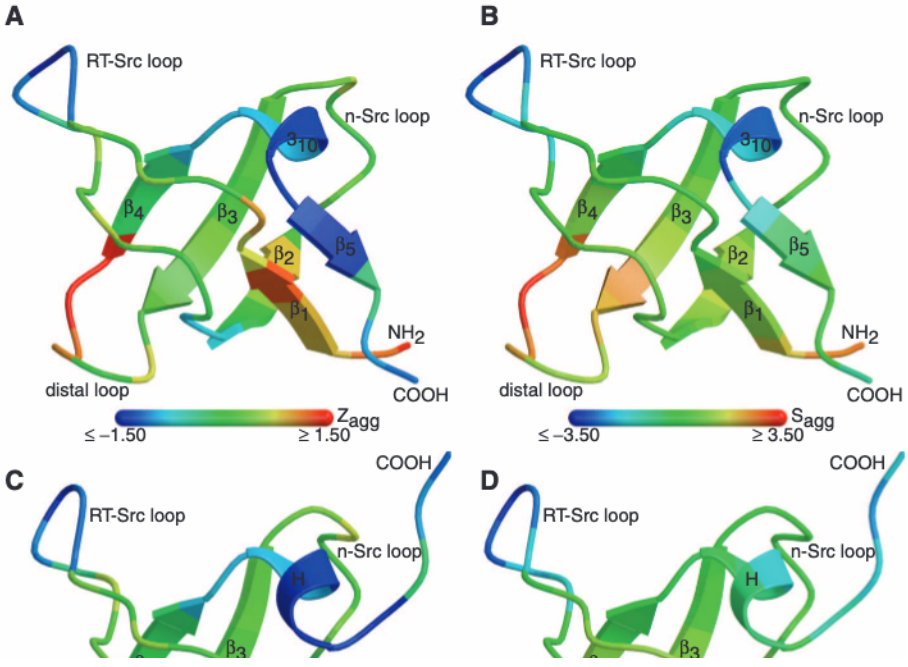

Fig. 2. Aggregation propensities of the native and intermediate states of A39V/N53P/V55L Fyn SH3. Sequence-based aggregation propensity score, Z_{agg} (*25*), color-coded onto the lowest-energy solution structure of (**A**) the native state and (**C**) the intermediate. Z_{agg} is normalized with respect to random sequences; $Z_{agg} > 1$ (orange to red) indicates significant propensity to aggregate. (**B**) Surface aggregation propensity score, S_{agg} (*32*), for the lowest-energy solution structure of the native state and (**D**) the intermediate.

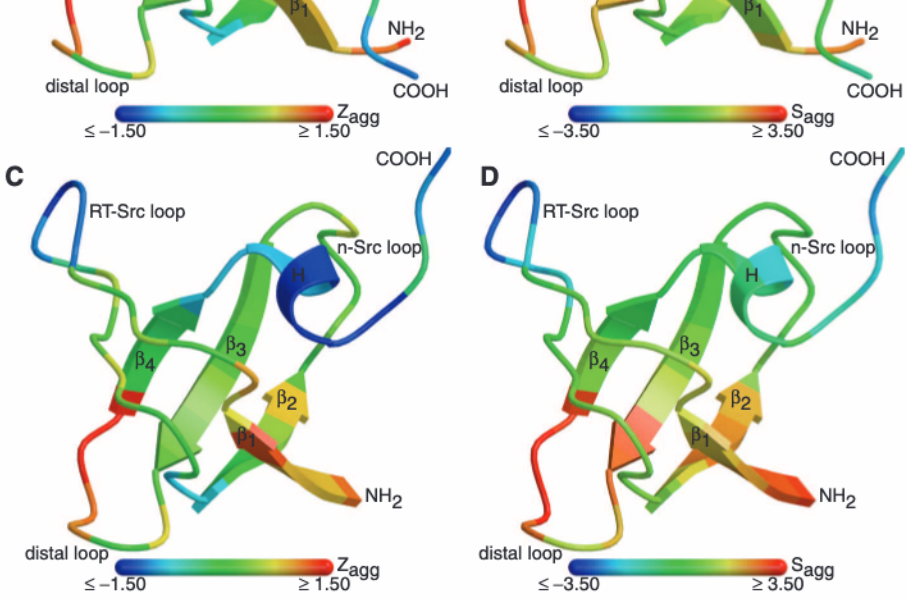
β1
NH2
distal loop
COOH
Zagg
≤ −1.50
≥ 1.50
β1
NH2
distal loop
COOH
Sagg
≤ −3.50
≥ 3.50

C
COOH
RT-Src loop
n-Src loop
H
β4
β3
β2
β1
NH2
distal loop
Zagg
≤ −1.50
≥ 1.50
D
COOH
RT-Src loop
n-Src loop
H
β4
β3
β2
β1
NH2
distal loop
Sagg
≤ −3.50
≥ 3.50

Our structure thus explains why the four-stranded β sheet constitutes a metastable folding intermediate. It also reveals how this state can lead to aggregation, as it exposes strand β_1, which has an unusually hydrophobic amino acid sequence that is predicted (*25*) to be aggregation-prone (Fig. 2, A and C). β sheets require nonideal edge strands to avoid aggregation (*26*), such as the bulge at Pro^{57} in strand β_5 of the native Fyn SH3 (Fig. 1C), a conserved structural feature at this position in SH3 domains. Accordingly, the native state is protected from aggregation (Fig. 2B), whereas the intermediate is highly aggregation-prone (Fig. 2D). Because the extent of aggregation of I is limited by its low population (≈2% of the total concentration), we have experimentally studied its aggregation propensity by engineering the truncation mutant, A39V/N53P/V55L/Δ(57-60) Fyn SH3. The truncated domain has the same temperature midpoint and enthalpy of folding (fig. S10) as predicted for I based on the thermodynamics of the A39V/N53P/V55L Fyn SH3 domain (*19*) and is a structural mimic of I, as verified by backbone chemical shifts (Fig. 3A, inset, and fig. S11).

As expected, A39V/N53P/V55L/Δ(57-60) Fyn SH3 spontaneously forms aggregates at room temperature under NMR conditions, associated with a significant resonance intensity loss on the time scale of days (Fig. 3A, top). This process can be slowed down dramatically by lowering the temperature (Fig. 3A, top), indicating a sizable rate-limiting energy barrier. This suggests that formation of stable aggregates after an initial oligomerization step may require extensive structural rearrangements. The resulting aggregates have a curly fibrillar shape with a diameter of several nanometers in negative-stain transmission electron micrographs (Fig. 3, B and C, and fig. S12, A to C). They exhibit characteristic amyloid-like properties: For example, they have a high β-strand content, as established by circular dichroism (CD) spectra that feature a very negative minimum at 214 nm in contrast with CD spectra of the native state (Fig. 3D), and they bind to Congo red dye (Fig. 3E and fig. S13A), a stain commonly used to identify amyloid deposits (*1*–*3*). Similar fibrillar aggregates are also formed by the truncation mutants Δ(56-60) and Δ(57-60) Fyn SH3 in the wild-type background (figs. S12, D to H, and S13, C and D). The aggregation observed here is specific only to the truncation mutants that were rationally designed on the basis of the intermediate-state structure (Fig. 3A, top). None of the other mutants we have studied previously (*22*) show any evidence for spontaneous aggregation under similar conditions (Fig. 3A, bottom), not even when the unfolded state populations are as high or higher than for the truncated domains examined above. These results provide strong evidence that aggregation does not proceed via global unfolding, but rather involves a locally unfolded state accessed through thermal fluctuations.

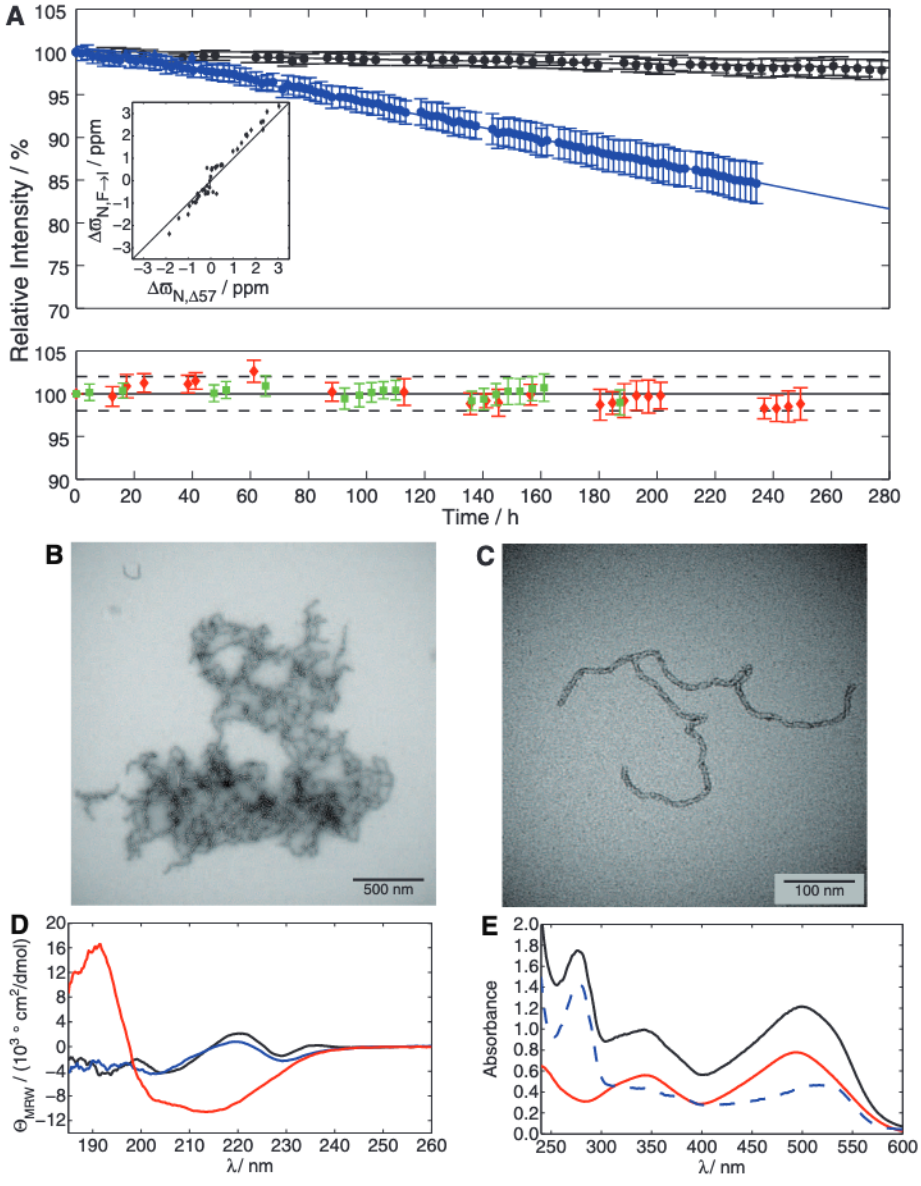

Fig. 3. Aggregation of the structural mimic of the folding intermediate. (**A**) Intensity loss of backbone amide resonances in a series of [^{1}H,^{15}N]–heteronuclear single quantum coherence spectroscopy experiments recorded on 1.0 mM [U-^{13}C,^{15}N] A39V/N53P/V55L/Δ(57-60) Fyn SH3 (top panel). Signal decreases of 0.16% per day at 15°C (black) and 1.6% per day at 20°C (blue) are quantified. The initial intensity (100%) is marked with a thick continuous horizontal line; sloped continuous lines are the result of linear regression. Monomeric A39V/N53P/V55L/Δ(57-60) Fyn SH3 predominantly adopts a structure mimicking the folding intermediate of the A39V/N53P/V55L Fyn SH3 domain [inset shows correlation between ^{15}N chemical shifts of I (*y* axis) and A39V/N53P/V55L/Δ(57-60) Fyn SH3 (*x* axis); fig. S11], with populations of the unfolded state estimated to be 5.7% at 15°C or 8.3% at 20°C (fig. S10). ppm, parts per million. In contrast, no significant systematic intensity loss could be detected for other destabilizing mutants (bottom panel) such as 0.9 mM L3A/A39V/N53P/V55L Fyn SH3 (red diamonds) (*22*) or 0.9 mM F20L/A39V/N53P/V55L Fyn SH3 (green squares) (*22*) at 35°C, even though the relative and absolute populations of the unfolded state under these conditions are similar (*22*) to those in the top panel. A threshold of 2% (dashed horizontal lines) was estimated to indicate a statistically significant change under the experimental conditions. Intensities are plotted as mean ± SD (error bars) over all backbone amide resonances that could be quantified accurately. (**B** and **C**) Negative stain transmission electron micrographs of A39V/N53P/V55L/Δ(57-60) Fyn SH3 showing aggregates at two different magnifications, as indicated by the scale bars. (**D**) Overlay of the CD spectra of A39V/N53P/V55L (black), A39V/N53P/V55L/Δ(57-60) Fyn SH3 monomers (blue), and aggregates (red). λ, wavelength; Θ_{MRW}, mean residue molar ellipticity. (**E**) Overlay of the absorption spectra of 20 μM Congo red in the absence (red) and presence (black) of A39V/N53P/V55L/Δ(57-60) Fyn SH3 aggregates. The difference spectrum (dashed blue curve) shows a clear hyperchromicity and red shift of the absorbance band around 500 nm.

Locally unfolded states that are separated from the N state by only low free-energy barriers play important roles in aggregation (*4*). In vivo or under physiological conditions, the structural fluctuations that access these locally destabilized conformers can be accelerated in a variety of ways, including by mutation, subunit dissociation, or cis-trans prolyl peptide bond isomerization (*4*, *11*, *12*). In vitro, fibril formation is often facilitated by destabilization through denaturants or acidic conditions, as in the case of the PI3K (*5*, *27*, *28*), α-spectrin (*29*, *30*), and Yes (*31*) SH3 domains. Interestingly, even under acidic conditions the aggregation propensity of an α-spectrin SH3 mutant was shown not to be correlated with overall stability (*29*), and thermodynamic measurements indicated that aggregation involved only partial unfolding (*30*), as observed for the Fyn SH3 domain studied here. In fact, many of the key residues and structural features that stabilize the A39V/N53P/V55L Fyn SH3 intermediate are also found in these other SH3 domains, suggesting that the mechanism of aggregation reported here is likely to be conserved. For example, Yes, N47A (Asn^{47}→Ala^{47}), α-spectrin, and PI3K SH3 domains all contain a hydrophobic side chain at the position corresponding to Phe^{4} in Fyn SH3 (Fig. 1D), as well as a hydrogen bond corresponding to the one between Ile^{28} HN and Thr^{2} CO (fig. S14) in the I state of the A39V/N53P/V55L Fyn SH3 domain, which compensates for the loss of interactions involving β_5 (Fig. 1C). Furthermore, the carboxyl-terminal region of strand β_5 is unfolded in amyloid-like PI3K SH3 fibrils (*27*, *28*), providing strong evidence in support of the conclusion that the formation of native strand β_5 is critical in preventing aggregation during folding.

Our study demonstrates that key processes leading to amyloid fibril formation can be understood through detailed structural studies of the monomeric precursors populated under close to physiological conditions. The three-dimensional structure of the SH3 domain intermediate reported here, obtained under native equilibrium conditions, provides a compelling illustration of how incomplete folding can trigger misfolding and aggregation. In this process, key non-native interactions that normally lead to folding also cause transient exposure of an aggregation-prone region subject to aberrant intermolecular association. These results highlight the promise of RD NMR for increasing our understanding of the link between thermally accessible, low-populated folding intermediates and fibril formation, as well as for the identification of specific structural elements that can be targeted through rational design of therapeutics against protein misfolding diseases.

References and Notes

1. C. M. Dobson, *Nature* **426**, 884 (2003).
2. D. J. Selkoe, *Nature* **426**, 900 (2003).
3. F. Chiti, C. M. Dobson, *Annu. Rev. Biochem.* **75**, 333 (2006).
4. F. Chiti, C. M. Dobson, *Nat. Chem. Biol.* **5**, 15 (2009).
5. M. Bucciantini *et al.*, *Nature* **416**, 507 (2002).
6. R. Tycko, *Annu. Rev. Phys. Chem.* **62**, 279 (2011).
7. V. N. Uversky, A. L. Fink, *Biochim. Biophys. Acta* **1698**, 131 (2004).
8. R. Kayed *et al.*, *Science* **300**, 486 (2003).
9. C. Haass, D. J. Selkoe, *Nat. Rev. Mol. Cell Biol.* **8**, 101 (2007).
10. R. Roychaudhuri, M. Yang, M. M. Hoshi, D. B. Teplow, *J. Biol. Chem.* **284**, 4749 (2009).
11. T. R. Jahn, M. J. Parker, S. W. Homans, S. E. Radford, *Nat. Struct. Mol. Biol.* **13**, 195 (2006).
12. C. M. Eakin, A. J. Berman, A. D. Miranker, *Nat. Struct. Mol. Biol.* **13**, 202 (2006).
13. A. Fersht, *Structure and Mechanism in Protein Science* (Freeman, New York, 1999).
14. A. P. Capaldi, S. E. Radford, *Curr. Opin. Struct. Biol.* **8**, 86 (1998).
15. A. G. Palmer 3rd, *Chem. Rev.* **104**, 3623 (2004).
16. P. Neudecker, P. Lundström, L. E. Kay, *Biophys. J.* **96**, 2045 (2009).
17. P. Vallurupalli, D. F. Hansen, L. E. Kay, *Proc. Natl. Acad. Sci. U.S.A.* **105**, 11766 (2008).
18. D. M. Korzhnev, T. L. Religa, W. Banachewicz, A. R. Fersht, L. E. Kay, *Science* **329**, 1312 (2010).
19. P. Neudecker *et al.*, *J. Mol. Biol.* **363**, 958 (2006).
20. A. Zarrine-Afsar *et al.*, *Proc. Natl. Acad. Sci. U.S.A.* **105**, 9999 (2008).
21. D. S. Riddle *et al.*, *Nat. Struct. Biol.* **6**, 1016 (1999).
22. P. Neudecker, A. Zarrine-Afsar, A. R. Davidson, L. E. Kay, *Proc. Natl. Acad. Sci. U.S.A.* **104**, 15717 (2007).
23. Y. Bai, *Chem. Rev.* **106**, 1757 (2006).
24. P. Robustelli, K. Kohlhoff, A. Cavalli, M. Vendruscolo, *Structure* **18**, 923 (2010).
25. G. G. Tartaglia *et al.*, *J. Mol. Biol.* **380**, 425 (2008).
26. J. S. Richardson, D. C. Richardson, *Proc. Natl. Acad. Sci. U.S.A.* **99**, 2754 (2002).
27. N. Carulla *et al.*, *Proc. Natl. Acad. Sci. U.S.A.* **106**, 7828 (2009).
28. M. J. Bayro *et al.*, *Biochemistry* **49**, 7474 (2010).
29. L. Varela, B. Morel, A. I. Azuaga, F. Conejero-Lara, *FEBS Lett.* **583**, 801 (2009).
30. B. Morel, L. Varela, A. I. Azuaga, F. Conejero-Lara, *Biophys. J.* **99**, 3801 (2010).
31. J. M. Martín-García, I. Luque, P. L. Mateo, J. Ruiz-Sanz, A. Cámara-Artigas, *FEBS Lett.* **581**, 1701 (2007).
32. S. Pechmann, E. D. Levy, G. G. Tartaglia, M. Vendruscolo, *Proc. Natl. Acad. Sci. U.S.A.* **106**, 10159 (2009).

Acknowledgments: We thank J. Forman-Kay and A. Davidson for providing laboratory space. S.S. and L.E.K. hold Canada Research Chairs in Biochemistry. P.R. was funded by a Gates Cambridge Scholarship and an NSF Graduate Research Fellowship, and P.W. is funded by a Natural Sciences and Engineering Research Council of Canada (NSERC) Canada Graduate Scholarship. This work was supported by grants from the NSERC and the Canadian Institutes of Health Research (L.E.K). The ensembles of 10 structures each representing the A39V/N53P/V55L Fyn SH3 domain native state from Ser^{1} to Asp^{59} and the folding intermediate from Ser^{1} to Ala^{56} have been deposited with the Protein Data Bank (accession codes 2LP5 and 2L2P, respectively).

Supplementary Materials

www.sciencemag.org/cgi/content/full/336/6079/362/DC1
Materials and Methods
Figs. S1 to S14
Tables S1 and S2
References (*33*–*111*)

20 September 2011; accepted 9 February 2012
10.1126/science.1214203